Nonlinear Dyn (2015) 82:1039–1058
DOI 10.1007/s11071-015-2216-9

ORIGINAL PAPER

Dynamic modeling and analysis of wear in spatial hard-on-hard couple hip replacements using multibody systems methodologies

Ehsan Askari · Paulo Flores · Danè Dabirrahmani · Richard Appleyard

Received: 1 December 2014 / Accepted: 13 June 2015 / Published online: 27 June 2015

Abstract Wear plays a key role in primary failure of artificial hip articulations. Thus, the main goal of this work is to investigate the influence of friction-induced vibration on the predicted wear of hard hip arthroplasties. This desideratum is reached by developing a three-dimensional multibody dynamic model for a hip prosthesis taking the spatial nature of the physiological loading and motion of the human body into account. The calculation of the intra-joint contact forces developed is based on a continuous contact force approach that accounts for the geometrical and materials properties of the contacting surfaces. In addition, the friction effects due to the contact between hip components are also taken into account. The vibration of the femoral head inside the cup associated with stick-slip friction, negative-sloping friction and dynamic variation in intra-joint contact force has been also incorporated in the present hip articulation model. The friction-induced vibration increases the sliding distance of the contact point between the head and cup surfaces by altering its micro- and macro-trajectories, and consequently affects the wear. In the present work, the Archard's wear law is considered and embedded in the dynamic hip multibody model, which allows for the prediction of the wear developed in the hip joint. With the purpose of having more realistic wear simulation conditions, the geometries of the acetabular cup and femoral head are updated throughout the dynamic analysis. The main results obtained from computational simulations for ceramic-on-ceramic and metal-on-metal hip prostheses are compared and validated with those available in the best-published literature. Finally, from the study performed in the present work, it can be concluded that an important source of the high wear rates observed clinically may be due to friction-induced vibration.

Keywords Wear simulation · Artificial hip articulation · Friction-induced vibration · Multibody dynamics

E. Askari (✉) · D. Dabirrahmani · R. Appleyard
Australian School of Advanced Medicine, Macquarie University, Sydney, NSW, Australia
e-mail: ehsanaskary@gmail.com

P. Flores
Departamento de Engenharia Mecânica, Universidade do Minho, Campus de Azurém, 4804-533 Guimarães, Portugal

1 Introduction

It is known that friction-induced vibration is an undesirable oscillation in artificial hip articulations due to tribological interactions between the head and cup surfaces, which eventually is a cause of wear. Ibrahim [1] showed that vibration induced by friction can lead to excessive wear of mechanical systems. Wear can also significantly influence the lifetime and performance of implants and has been found to be a crucial factor in primary failure of artificial hip replacements [2].

The most commonly utilized artificial hip replacement combination is a metal head within a polymer cup, which is usually referred to as a soft-on-hard couple.

This pair of materials is known to suffer from cup wear with the resultant polymer debris reported to induce osteolysis. Computing the wear profile of soft-on-hard bearing couples has been the subject of a good number of studies over the last decades [3–8]. With the intent to reduce wear, hard-on-hard material combinations have been developed namely metal-on-metal (MoM) and ceramic-on-ceramic (CoC) bearings. In the case of hard-on-hard couples, wear occurs across both the head and cup surfaces. Few studies have investigated wear of hard-on-hard couples [9–11].

Hip simulator tests have been developed to evaluate implant wear; however, these tests are time-consuming and costly [9,12,13]. Therefore, significant effort has been placed on developing computational wear models [3,4,11]. While a number of computational approaches have been proposed to predict wear and friction phenomena [14,15], Archard's wear law is still the most commonly utilized in tribology [14–18]. This wear model requires knowledge of the contact pressure, sliding distance of the contact point and tribological data, such as the wear coefficient of the contacting materials. Implant head-cup contact properties can be numerically determined by means of the finite element method [19], boundary element method [2] and Hertz contact model [20,21]. Each has its advantages and disadvantages in terms of accuracy and computational efficiency; for instance, it has been recognized that the finite element method provides more accurate results, but it is more time-consuming [16].

The contact point between the head and cup surfaces follows a certain characteristic track during normal human gait. The contact point track is a crucial parameter to predict the wear, since any variation in the track shape can cause a huge difference in the wear rate [22–24]. Mattei et al. [8] utilized a theoretical contact point track, where the contact point was assumed to be located at the interface of the head and cup and along the line joining both the centers of the head and cup. Jourdan and Samida [4] considered that the center of the femoral head was stationary, while the motion of the femur was simulated by applying physiological rotations. Ramamuri and his co-authors [25] computationally determined loci of movement of selected points on the femoral head during normal gait. A few years later, Saikko and Calonius [26] developed a computational method based on Euler angles to compute the slide tracks for the three-axis motion of the hip articulation in walking. The slide track patterns resulting from the gait waveforms were found to be similar to those produced by hip simulators. More recently, Sariali and his co-workers [27] also provided sliding path of motion between the head and cup when the hip implant is in edge loading or in normal centered conditions using the Leeds II hip simulator.

The geometry of the hip contacting surfaces changes as wear progresses over time, which, in turn, affect contact pressure and nominal contact zone/point. From this point of view, the wear prediction procedures can be classified into two main groups. In the first group, it is assumed that surface geometries and, consequently, contact pressures and sliding distance do not change over the wear simulation [8]. As a result, a linear extrapolation can be applied to estimate the final linear and volumetric wear. This procedure is very efficient from computational point of view, but has been found to produce erroneous results [16,28]. In sharp contrast, the second group allows the contact geometry to vary gradually and, thus, result in iterative procedures to compute wear and final geometry [10]. Thus, the surface geometry is changing due to wear and, consequently, increases the joint clearance size and modifies the contacting areas from uniform to nonuniform. Therefore, the contact pressure and the dynamic response of the system can significantly be affected.

Recently, investigations have been reported that, on top of the normal gross motion, the femoral head vibrates inside the cup with micron and nanoamplitudes in tangential and normal directions, respectively, with respect to the collision plane due to friction-induced vibration [29,30]. This results in a change in the contact point trajectory at both micro- and macroscales, which can affect the final wear profile. Mattei and Di Puccio [11] determined the variations of contact point trajectory due to friction and calculated its effect on wear prediction. This approach does not include the vibration of the femoral head inside the cup. In addition, it is reported that wear decreased as friction increased, which is not acceptable from physical point of view. To the best of the authors' knowledge, there is no investigation on the effect of the vibration of the femoral head within the cup on both wear prediction and the corresponding wear map of artificial hip joints. Moreover, the authors' previous work demonstrated that friction modifies the smooth trajectory of the head moving against the cup to a nonsmooth oscillatory trajectory with an oscillatory sliding path [31]. Consequently, a significant wear increase should be expected.

Thus, the influence of friction-induced vibration on wear simulation of artificial hip articulations is modeled and analyzed in this study. For this purpose, a spatial multibody dynamic model is developed, which allows for the evaluation of both sliding distance and contact pressure in order to evaluate the wear of hip implants. The friction-induced vibration and intra-joint contact-impact forces developed between the head and cup surfaces are evaluated and taken into consideration as external generalized forces in the governing equation of the motion [32]. A friction–velocity relation and a dissipative Hertz contact model are employed to formulate tangential and normal contact forces, respectively [33]. Three-dimensional physiological loading and motion of the human body are also taken into account in the dynamic analysis [34]. Then, the resulting nonlinear equations of motion are solved by using the adaptive Runge–Kutta–Fehlberg method. In this process, the Archard's law is utilized to compute the wear, being the geometry of worn hip surfaces updated during the computational simulation. Finally, demonstrative examples of application are utilized to provide the results that support the discussion and show the validity of the presented methodology. For the sole purpose of validation, the obtained results are also analyzed and compared with those available in the thematic literature.

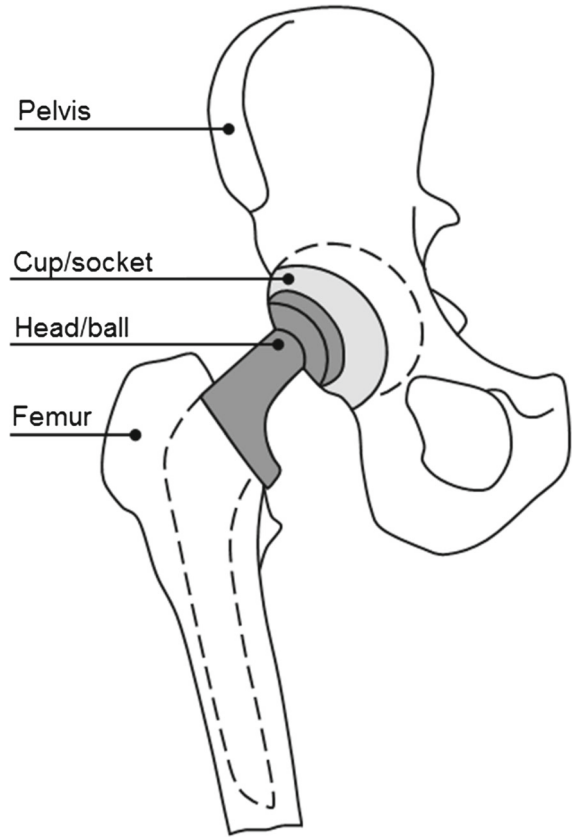

Fig. 1 Schematic representation of the artificial hip replacement

2 General issues on modeling artificial hip joints

The main purpose of this section is to present the fundamental issues dealing with the development of a computational multibody hip model able to predict the wear in human artificial hip joints. The hip articulation, also referred to the acetabulofemoral joint, is one of the most significant synovial joints in the human body. This joint connects the femur and acetabulum of the pelvis. It has two main functions: (*i*) to provide static stability and (*ii*) to permit the motion during human gait [35]. The mobility associated with the hip joint is indispensable to human locomotion. There is no doubt that the hip joint is one of the most studied human anatomical articulations due to its importance in activities of daily living and due to high incidence of joint degeneration, which ultimately can lead to serious disability and affect the human gait [36–38]. Figure 1 shows a schematic representation of an artificial hip replacement, where the main components are the femoral head (ball) and the acetabular cup (socket).

The human body has relatively rigid bones, connected by special joints capable of large anatomical articulations. From a mechanical point of view, this description of the human body is similar to that of a multibody mechanical system. However, the human body system is far more complex than the great majority of the multibody systems. Its components have a complex behavior due to deformations associated with the soft tissues such as the muscles, tendons and ligaments and due to the complexity of the anatomical articulations relative to the standard mechanical joints [39]. Multibody-based methodologies have been developed in such a way that, besides the representation of mechanical systems made only of rigid components [32], they also allow the description of deformable bodies [40]. In a broad sense, much of the research developed with the purpose to simulate daily human tasks is based on the assumption that the joints that con-

strain the system's components are considered as ideal or perfect joints, such as spherical, revolute and universal joints. Nevertheless, with this approach significant decrease in the kinematic and dynamic precision compared with the living body can occur because the idealized models fail to capture more complex aspects of joint kinematics and dynamics [41].

In the field of multibody system dynamics, computational methods for representation of complex phenomena such as contact geometry, friction phenomena, wear and lubrication have been developed [42]. However, the application of these methods in the field of biomechanical system dynamics lacks somewhat behind. A possible reason is that much biomechanical simulation is based upon inverse dynamics, where movement of all degrees of freedom is input to the analysis leading to a presumption of simple joint kinematics. For most applications concerning simple models, this is a reasonable assumption, but for detailed investigations of more complex joints, such as the artificial hips it is not. In contrast, in the present study, a dynamic model of the artificial hip joint is considered, in which the head and cup are modeled as contacting components [43]. The biomechanical hip model characterization is developed under the framework of multibody system methodologies using Cartesian coordinates. The intra-joint forces associated with the impacts and the eventual continuous contacts are described here by a force model that accounts for the geometric and material characteristics of the head and cup surfaces. The model for the contact-impact force must consider the material and geometric properties of the colliding surfaces, information on the impact velocity, contribute to an efficient integration and account for some level of energy dissipation [44]. These forces are then included into the equations of motion as generalized external forces. In this process, the Archard's law is embedded in the general dynamic multibody approach proposed.

3 Kinematics of artificial hip joints

In order to describe the kinematic aspects of an artificial hip joint, it is first necessary to formulate a mathematical model. In the present work, the biomechanical characterization is developed under the framework of multibody systems methodologies. Due to its simplicity and computational easiness, Cartesian coordinates and Newton–Euler method are utilized to formulate the equations of motion of the three-dimensional multibody hip model [32]. From the multibody point of view, a hip joint can be modeled as a spherical joint with clearance, as Fig. 2 shows [43]. The femoral head is the ball, while the acetabular cup is the socket. The ball is part of body j, which is inside the hemisphere cup that is part of body i. The radii of the head and cup are R_j and R_i, respectively. The difference in radius between the cup and head defines the size of radial clearance in the hip joint, $c = R_i - R_j$. In the present study, the centers of mass of bodies i and j are O_i and O_j, respectively. Body-fixed coordinate systems $\xi\eta\zeta$ are attached at their centers of mass, while XYZ represents the global inertial frame of reference. Point P_i indicates the center of the cup, while the center of the head is denoted by P_j. The vector that connects the point P_i to point P_j is defined as the eccentricity vector, which is represented in Fig. 2. It should be noticed that, in actual hip joints, the magnitude of the eccentricity is typically much smaller than the radius of the socket and ball [45].

In what follows, the fundamental kinematic aspects related to the hip joint are presented. As displayed in Fig. 2, the eccentricity vector $\mathbf{e}$, which connects the centers of the cup and the head, is expressed as

$$\mathbf{e} = \mathbf{r}_j^P - \mathbf{r}_i^P \tag{1}$$

where both $\mathbf{r}_j^P$ and $\mathbf{r}_i^P$ are described in global coordinates with respect to the inertial reference frame [32],

$$\mathbf{r}_k^P = \mathbf{r}_k + \mathbf{A}_k \mathbf{s}'^P_k, \quad (k = i, j) \tag{2}$$

The magnitude of the eccentricity vector is evaluated as,

$$e = \sqrt{\mathbf{e}^T \mathbf{e}} \tag{3}$$

The magnitude of the eccentricity vector expressed in the global coordinates is written as [46],

$$e = \sqrt{\left(x_j^P - x_i^P\right)^2 + \left(y_j^P - y_i^P\right)^2 + \left(z_j^P - z_i^P\right)^2} \tag{4}$$

and the time rate of change of the eccentricity in the radial direction, that is, in the direction of the line of centers of the socket and the ball is,

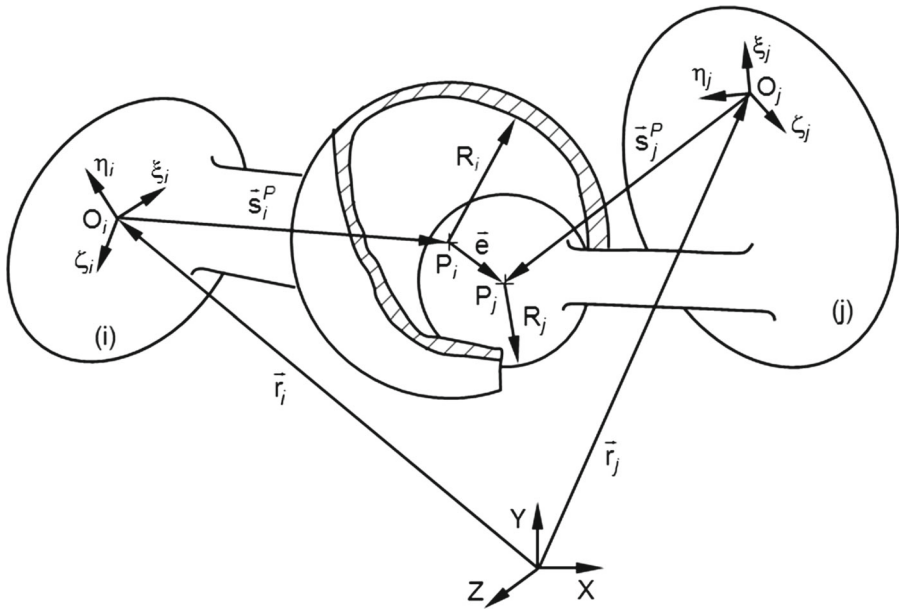

Fig. 2 General configuration of an artificial hip joint in a multibody systems [46]

$$\dot{e} = \frac{(x_j^P - x_i^P)\left(\dot{x}_j^P - \dot{x}_i^P\right) + \left(y_j^P - y_i^P\right)\left(\dot{y}_j^P - \dot{y}_i^P\right) + \left(z_j^P - z_i^P\right)\left(\dot{z}_j^P - \dot{z}_i^P\right)}{e} \tag{5}$$

in which the dot denotes the derivative with respect to time.

A unit vector $\mathbf{n}$ normal to the collision surface between the socket and the ball is aligned with the eccentricity vector, as observed in Fig. 2. Thus, it can be stated that

$$\mathbf{n} = \frac{\mathbf{e}}{e} \tag{6}$$

Figure 3 illustrates the situation in which the cup and the head surfaces are in contact, which is identified by the existence of a relative penetration, δ. The contact or control points on bodies i and j are Q_i and Q_j, respectively. The global position of the contact points in the cup and head is given by [46,47],

$$\mathbf{r}_k^Q = \mathbf{r}_k + \mathbf{A}_k \mathbf{s}_k'^Q + R_k \mathbf{n}, \quad (k = i, j) \tag{7}$$

where R_i and R_j are the cup and head radius, respectively.

The velocities of the contact points Q_i and Q_j in the global system are obtained by differentiating Eq. (7) with respect to time, yielding,

$$\dot{\mathbf{r}}_k^Q = \dot{\mathbf{r}}_k + \dot{\mathbf{A}}_k \mathbf{s}_k'^Q + R_k \dot{\mathbf{n}}, \quad (k = i, j) \tag{8}$$

Let the components of the relative velocity of contact points in the normal and tangential direction to the surface of collision represented by $\mathbf{v}_\mathrm{N}$ and $\mathbf{v}_T$, respectively. The relative normal velocity determines whether the surfaces in contact are approaching or separating, and the relative tangential velocity determines whether the surfaces in contact are sliding or sticking [48]. The relative scalar velocities, normal and tangential to the surface of collision, v_N and v_T, are obtained by projecting the relative impact velocity onto the tangential and normal directions, yielding,

$$\mathbf{v}_N = [(\dot{\mathbf{r}}_j^Q - \dot{\mathbf{r}}_i^Q)^T \mathbf{n}]\mathbf{n} \tag{9}$$

$$\mathbf{v}_T = (\dot{\mathbf{r}}_j^Q - \dot{\mathbf{r}}_i^Q)^T - \mathbf{v}_N \equiv v_T \mathbf{t} \tag{10}$$

where $\mathbf{t}$ represents the tangential direction to the impacted surfaces.

From Fig. 3, it is clear that the geometric condition for contact between the socket and ball can be defined as,

$$\delta = e - c \tag{11}$$

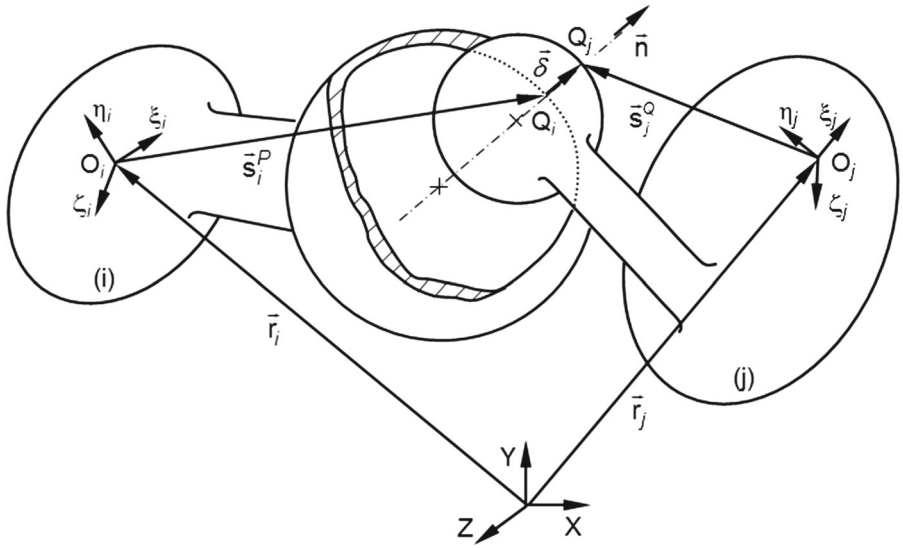

Fig. 3 Penetration depth between the cup and the head during the contact [46]

where e is the magnitude of the eccentricity vector given by Eq. (3) and c is the radial clearance. It should be noted that here the clearance is taken as a specified parameter. When the magnitude of the eccentricity vector is smaller than the radial clearance, there is no contact between the cup and the head, and consequently, they can freely move relative to each other. When the magnitude of eccentricity is larger than radial clearance, there is contact between the cup and head, being the relative penetration given by Eq. (11).

The contact problem studied within the framework of multibody systems formulations can be divided into two main phases, namely (*i*) the contact detection and (*ii*) the application of an appropriate contact force law [49]. The contact detection is the procedure which allows to check whether the potential contacting surfaces are in contact or not. For multibody systems, this analysis is performed by evaluating, at each integration time step, the gap or distance between contacting points. When this distance is negative, it means that the bodies overlap, and hence in these situations, the distance is designated as penetration or indentation. In reality, the bodies do not penetrate each other, but they deform. In computational simulations, the penetration is related to the actual deformation of the bodies [50]. On the other hand, in the second phase of the contact modeling problems, the application of the contact law deals with the use of an appropriate constitutive law relating the penetration and the contact forces necessary to avoid the inter-penetration of the contacting bodies. In other words, the contact force can be thought of penalizing the pseudo-penetration, and hence, this approach is commonly denominated as penalty method [51–55].

4 Dynamics of artificial hip joints

In the present study, the dynamics of the artificial hip joint is done by employing the Newton–Euler equations of motion for unconstrained systems, which can be expressed as [32]

$$\mathbf{M}\ddot{\mathbf{q}} = \mathbf{g} \tag{12}$$

where $\mathbf{M}$ is the system mass matrix, containing the mass and moment of inertia of the femoral and cup elements, $\ddot{\mathbf{q}}$ denotes the vector of the translational and rotational accelerations, and $\mathbf{g}$ is a force vector that includes the external and Coriolis forces acting on the components of the multibody hip system. The external forces represent the intra-joint contact forces as well as the moments that act on the hip joint. The numerical resolution of Eq. (12) is performed using the adaptive Runge–Kutta–Fehlberg method and the state representation to convert the second-order differential equations into first-order equations [56].

When the head and cup surfaces contact each other, normal and tangential forces are developed at the contact points, Q_i and Q_j. On the one hand, these intra-joint contact forces do not act through the center of mass of the bodies i and j, and the moment components for

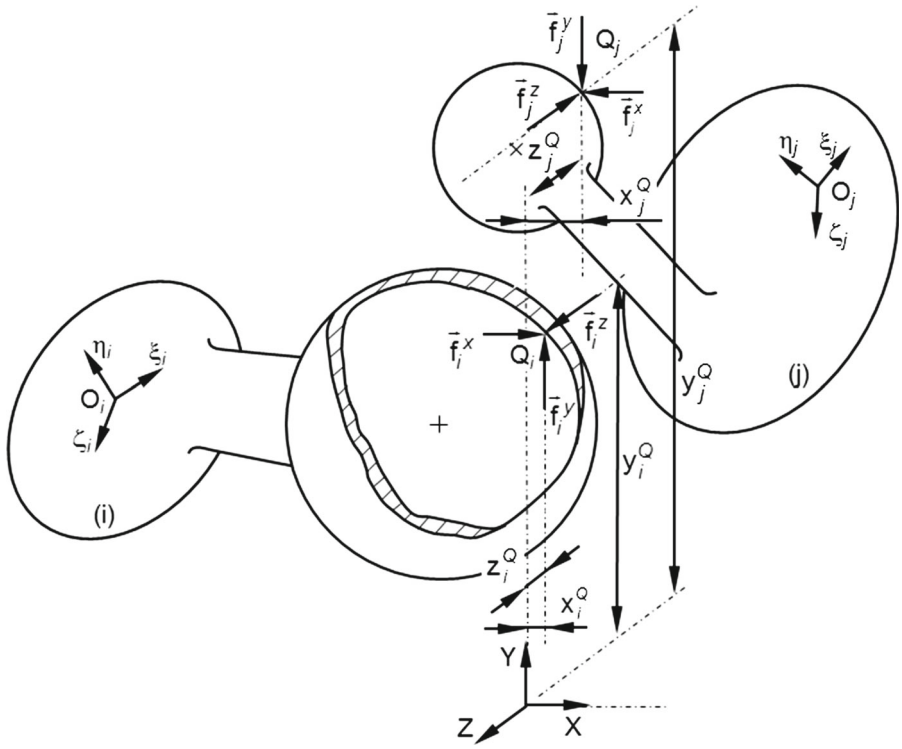

Fig. 4 Contact forces defined at the points of contact between cup and head [46]

each body need to be determined. On the other hand, the contribution of the contact forces to the generalized vector of forces is found by projecting the normal and tangential forces onto the X, Y and Z directions. Based on Fig. 4, the equivalent forces and moments working on the center of mass of body i (the cup element) are given by

$$\mathbf{f}_i = \mathbf{f}_N + \mathbf{f}_T \tag{13}$$

$$\mathbf{m}_i = \tilde{\mathbf{s}}_i^Q \mathbf{f}_i \tag{14}$$

where tilde ($\sim$) placed over a vector indicates that the components of the vector are used to generate a skew-symmetric matrix [32].

The forces and moments acting on body j (the femoral head) are written as

$$\mathbf{f}_j = -\mathbf{f}_i \tag{15}$$

$$\mathbf{m}_j = -\tilde{\mathbf{s}}_j^Q \mathbf{f}_i \tag{16}$$

At this stage, it must be stated that due to muscle activities, other soft tissues and leg motion, there are other external forces and moments acting on the center of the femoral head from which forces are available from in vivo data. However, moments are unknown, which should be computed in a way that the femoral head satisfies its in vivo motions. The moments express the dependency of normal contact forces and tangential friction forces in the collision plane.

The normal contact forces are computed considering the well-known viscoelastic model proposed by Lankarani and Nikravesh [57]. This continuous contact force model, in which a hysteretic damping factor is incorporated in order to account for the energy dissipation, is expressed as

$$f_N = K\delta^n \left[1 + \frac{3\left(1 - c_e^2\right)}{4} \frac{\dot{\delta}}{\dot{\delta}^{(-)}}\right] \tag{17}$$

where K is the generalized stiffness parameter, n is the nonlinear exponent, c_e is the coefficient of restitution, $\dot{\delta}$ is the relative penetration velocity and $\dot{\delta}^{(-)}$ is the initial impact velocity. Equation (17) is used to simulate the impact because it accounts for energy dissipation and exhibits good numerical stability at low impact velocities. Moreover, Eq. (17) is valid for impact velocities lower than the propagation speed of elastic waves across the bodies. This criterion is fulfilled in the applications used in the present study. In fact, with low values of clearance size, the impact velocities in the hip joint are within a tolerable range of validity of the

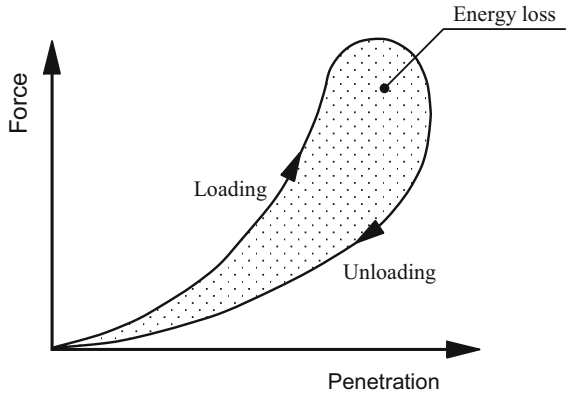

Fig. 5 Force versus penetration [57]

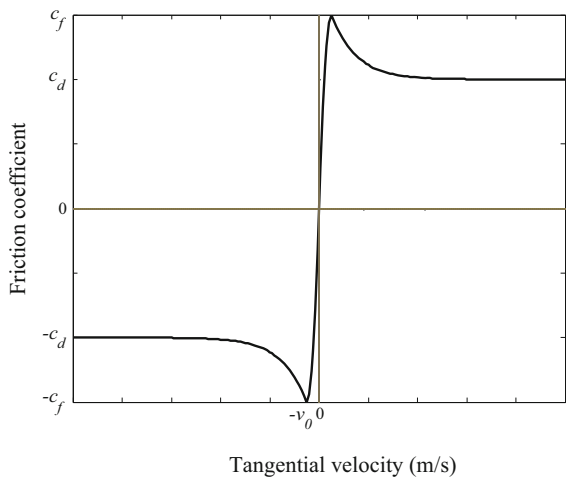

Fig. 6 Coefficient of friction behavior as a function of the relative tangential velocity [31,63]

contact force model given by Eq. (17) [58]. The generalized stiffness parameter K depends on the geometry and mechanical properties of the contacting surfaces. For two spherical contacting bodies with radii R_i and R_j, the stiffness parameter is expressed by [59]

$$K = \frac{4}{3(\sigma_i + \sigma_j)} \sqrt{\frac{R_i R_j}{R_i - R_j}} \tag{18}$$

in which the material parameters σ_i and σ_j are given by

$$\sigma_l = \frac{1 - \upsilon_l^2}{E_l}, \quad (k = i, j) \tag{19}$$

and the quantities υ_l and E_l are the Poisson's ratio and the Young's modulus associated with each sphere, respectively. It is important to note that, by definition, the radius is negative for concave surfaces (such as for the head element) and positive for convex surfaces (such as for the cup element) [60].

The force expressed by Eq. (17), when drawn versus penetration depth, results in a hysteresis loop as shown in Fig. 5. The area of this hysteresis loop is equal to the energy loss due to the internal damping of the material. The hysteresis damping function assumes that the loss in energy during impact is due to the material damping of the colliding bodies [57]. Alternative contact force models are available in the literature [33].

The tangential friction is evaluated by using the modified Coulomb's friction law [61]

$$f_T = -\mu(v_T) f_N \tag{20}$$

where v_T denotes the relative tangential velocity and μ represents the coefficient of friction. Although the coefficient of friction is dependent on several parameters, in the present study, it is constricted to dependence on the relative tangential velocity as

$$\mu(v_T) = \begin{cases} \left(-\frac{c_f}{v_0^2}(v_T - v_0)^2 + c_f\right) \operatorname{sgn}(v_T) & v_T < v_0 \\ \left(c_d + (c_f - c_d)\exp\left(-\xi(v_T - v_0)\right)\right) \operatorname{sgn}(v_T) & v_T \geq v_0 \end{cases} \tag{21}$$

in which c_f and c_d are the static and dynamic coefficients of friction, respectively, v_0 is the tolerance velocity utilized to avoid numerical instabilities when the relative tangential velocity is close to zero and ξ (greater than zero) denotes the negative slope of sliding state [62]. It must be highlighted that the first equation in (21) reflects the continuous behavior of the coefficient of friction when the relative tangential velocity is the vicinity of zero, while the second equation in (21) represents the Stribeck friction component. With the purpose to make clear the complex function of Eq. (21), Fig. 6 shows the evolution of the coefficient of friction as a function of the relative tangential velocity. It must be stated that the coefficient of friction starts from zero, and it drastically increases reaching a peak, which has been referred to as static friction by Bengisu and Akay [63]. Then, the coefficient of friction will increase with relative tangential velocity until reaching a stable response.

5 Modeling wear in artificial hip joints

This section deals with the main issues associated with modeling wear in artificial hip joints. For this purpose, the Archard's wear approach is utilized, in which the linear wear rate can be expressed as follows [22],

$$\frac{\mathrm{d}h}{\mathrm{d}s} = \frac{K_W p}{H} \tag{22}$$

where h represents the depth wear, s is the sliding distance, K_W denotes the dimensionless wear coefficient, p represents the contact pressure and H is the hardness of the softer material of the contact pair elements. A numerical solution for the wear depth, given by Eq. (22), can be obtained by employing the Euler integration algorithm, yielding the following updating expression

$$h_{i+1} = h_i + k_W p_i \Delta s_i \tag{23}$$

in which h_{j+1} is the total wear up to the $j+1$th wear step, h_j is the total wear depth at the previous step. The last term in Eq. (23) is the incremental wear depth, which is a function of the contact pressure and the incremental sliding distance at the corresponding cycle. Finally, the variable k_W denotes the wear coefficient ($k_W = K_W/H$), which is dimensionally defined as $\mathrm{mm}^3/\mathrm{N\,m}^{-1}$. As it can be observed from Eq. (23), sliding distance (Δs_i) and contact pressure (p_i) in each step of the simulation should be evaluated before the computation of wear. Thus, the sliding distance can be calculated from the numerical solution of Eq. (12), in each time step, and can be expressed in the following form

$$\Delta s_i = \sqrt{(x_j^Q(t_i) - x_j^Q(t_{i-1}))^2 + (y_j^Q(t_i) - y_j^Q(t_{i-1}))^2 + (z_j^Q(t_i) - z_j^Q(t_{i-1}))^2} \tag{24}$$

It should be mentioned that Eq. (24) can precisely represent the sliding distance increment provided that the time step is enough small.

The Hertzian contact theory can be utilized to estimate the contact parameters such as the maximum pressure and contact area. Assuming that the cup and head to be held in contact by a force f_N such that their point of contact expands into a circular area of radius a

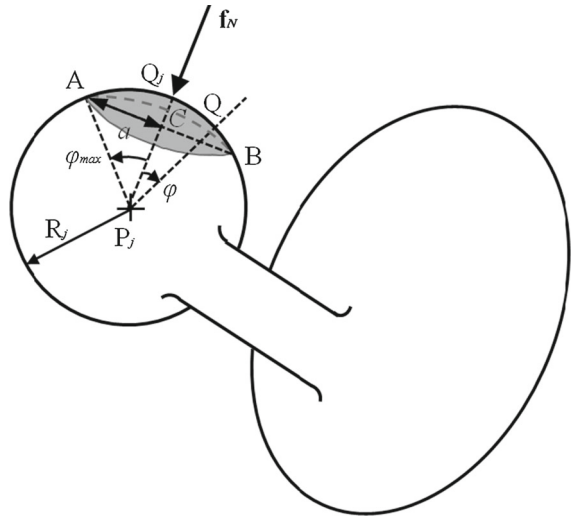

Fig. 7 A representation of contact area and the contact angle φ

$$a = K_a \sqrt[3]{f_N} \tag{25}$$

where

$$K_a = \sqrt[3]{\frac{3}{4}\frac{(\sigma_i + \sigma_j)\, R_i R_j}{R_i - R_j}} \tag{26}$$

in which σ_i, σ_j, R_i and R_j have already been defined in the context of Eq. (18). The maximum contact pressure, $p_{\max}$, occurs at the center point of the contact area with a magnitude given by

$$p_{\max} = \frac{3 f_N}{2\pi a^2} \tag{27}$$

Based on the Hertzian contact theory, the pressure field at any point within the contact point area can be expressed in the following form [64]

$$p(\varphi) = p_{\max}\sqrt{1 - \left(\frac{\sin\varphi}{\sin\varphi_{\max}}\right)^2} \tag{28}$$

where $\varphi_{\max}$ can be obtained from the geometry of Fig. 7, yielding

$$\sin\varphi_{\max} = \frac{a}{R_j} \tag{29}$$

According to Fig. 7, φ is the angle defined between the vectors, $\overrightarrow{P_jQ_j}$ and $\overrightarrow{P_jQ}$, in which Q is an arbitrary point within the contact area displayed in gray color. Using the scalar product between those vectors results in Eq. (30) by which φ can be evaluated. The same procedure can be considered for the angle φ' on the cup surface, yielding

$$\overrightarrow{P_jQ}\,\overrightarrow{P_jQ_j} = R_j^2 \cos\varphi \tag{30}$$

$$\overrightarrow{P_iQ} \cdot \overrightarrow{P_iQ_i} = R_i^2 \cos\varphi' \tag{31}$$

At this stage, it must be noted that when $\varphi > \varphi_{\max}$ on the head surface, the pressure of the corresponding point is zero. Otherwise, the pressure is calculated from Eq. (28).

The geometry of the cup and head surfaces should be updated during simulation due to material loss. Updating the geometry of the cup is straightforward since the cup is assumed to be stationary. On the other hand, the head freely moves due to the leg movement from which there are available clinical data of its physiological rotation over the gait cycle. Consequently, the local coordinate system attached to the center of the ball rotates with respect to the reference coordinate system to the angles (α, β, γ), which are Euler angles represented in the plots of Fig. 8. Thus, in order to update the geometry of the head, each point in the contact area determined in the reference coordinate system is transferred to the local coordinate system. This helps to determine the exact position of the point on the ball surface, which is different from what is in the reference coordinate system due to using different coordinate systems. For this purpose, the position of the contact point on the head surface can be determined using the following standard transformation

$$\mathbf{Q}_{j_0} = \mathbf{R}_{xyz}^{-1}(\alpha, \beta, \gamma)\mathbf{Q}_j \tag{32}$$

where $\mathbf{Q}_{j0}$ is the local position of contact point in local coordinate system and $\mathbf{Q}_j$ is the position of the contact point in the global coordinate system. Moreover, $\mathbf{R}_{xyz}$ is the rotation matrix, for which the Euler sequence FE-AA-IER (i.e., FE: flexion–extension; AA: abduction–adduction; IER: internal–external rotation) is given by [65]

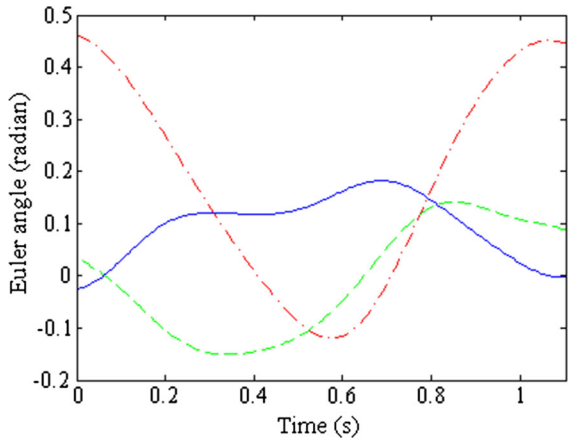

Fig. 8 The Euler angles due to the physiological motion of the femoral head where *solid line* γ(IER); *dashed lines* β(AA); *dash-dotted lines* α (FE) [34]

In order to compute the exact area covered by the sliding distance, the joint surface is divided into several elements before starting the dynamic simulation. Discretizing the head and cup surfaces, the azimuthal and polar angles of the spherical coordinate systems at the center of the head and cup are differential angles with the size $\pi/\varkappa$ radian, where $\varkappa$ is an integer. Consequently, the elements are not uniform and the accuracy of the results and convergence of the method are assessed with increasing $\varkappa$. This particular issue will be discussed in detail in the next sections of the paper. Figure 9 shows a representation of two potential contact surfaces discretized into finite elements and elements involved in contact. It is worth mentioning that finite element method is not used in the present study and contact pressure is determined in the exact location of the contact point using Eq. (28). Thus, the contact area covers a number of elements in which contact pressure is positive. The wear depth in each element (k, j) covered by contact area changes according to the Archard's wear model. In each integration time step, when the contact between two surfaces occurs, the wear depth calculated for each element is stored. At the end of the simulation, the amount of wear depth accumulated on an element is the sum of all partial wear depths at

$$\mathbf{R}_{xyz}(\alpha, \beta, \gamma) = \begin{bmatrix} \cos\beta\cos\gamma & -\cos\beta\sin\gamma & \sin\beta \\ \sin\alpha\sin\beta\cos\gamma + \cos\alpha\sin\gamma & -\sin\alpha\sin\beta\sin\gamma + \cos\alpha\cos\gamma & -\sin\alpha\cos\beta \\ -\cos\alpha\sin\beta\cos\gamma + \sin\alpha\sin\gamma & \cos\alpha\sin\beta\sin\gamma + \sin\alpha\cos\gamma & \cos\alpha\cos\beta \end{bmatrix} \tag{33}$$

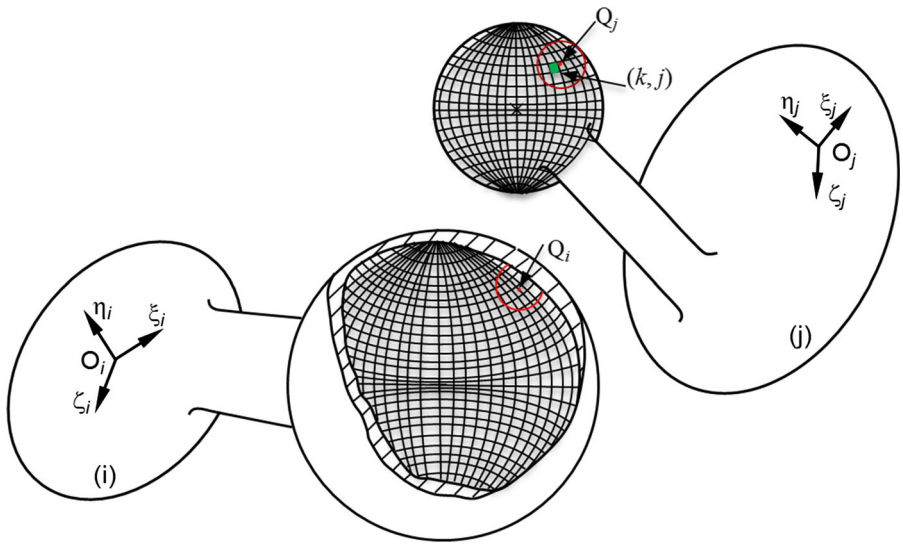

Fig. 9 A representation of finite element on the cup and head surface in which Q_j and Q_i are contact points on the head and cup, respectively, that placed at the center of their contact area within the circles in red color. The green block shows one element (k, j) engaged in the contact area

each time step. With this methodology, it is possible to compute the new geometric configuration of the joint surface caused by wear. The total amount of wear depth can be expressed by [14]

$$h^T_{(k,j)} = \sum_{1}^{n} h_{(k,j)}(t_i) \tag{34}$$

where (k, j) represents the row and column numbers of a surface element and the summation is done with respect to the number of time steps from 1 to n.

Finally, after the calculation of wear depth at each time step, the cup and head radii of any element involved in contact are updated as follows

$$R_j^{(k,j)}(t_i) = R_j^{(k,j)}(t_{i-1}) - \frac{h_{(k,j)}(t_i)}{2} \tag{35}$$

$$R_i^{(l,m)}(t_i) = R_i^{(l,m)}(t_{i-1}) + \frac{h_{(k,j)}(t_i)}{2} \tag{36}$$

where $R_j^{(k,j)}(t_i)$ and $R_i^{(l,m)}(t_i)$ are the head and cup radii of the element (k, j) on the head surface and (l, m) on the cup surface at the time (t_i). In the present work, it is assumed that the element (k, j) of the head articulates the element (l, m) of the cup at this time step. The quantity $h_{(k,j)}(t_i)$ represents the amount of wear depth computed for the articulation constituted by these two elements. From the analysis of Eqs. (35) and (36), it is assumed that the amount of wear at each time step is uniformly distributed between two elements articulating against each other, one on the cup surface and another on the head, as half of the total wear depth.

6 Results and discussion

The main objectives of this investigation were to investigate the effect of friction-induced vibration on predicted wear of artificial hip joints and to study high wear rates seen in vivo for noisy CoC hip implants. The resulting equations of the Archard's wear model integrated into the multibody dynamic formulation of artificial hip joints were numerically solved using the adaptive Runge–Kutta–Fehlberg method to discretize the interval of time of analysis [31]. To acquire accurate and stable outcomes, an error threshold was defined. At each time step of dynamic simulation, the error magnitude was assessed by comparing results obtained from explicit method with different orders. When the error magnitude was greater than the error threshold, the time step is halved and computation redone. In this process, the minimum value for the integration step size was considered to be 0.0000001s and the corresponding integration tolerance 0.00000001. Hip prostheses tested in the present study had the following geometric properties: the femoral head radius equal to 14 mm and radial clearance 50 μm. Material parameters of the bearing couples were as follows: Al_2O_3 ceramic with a Young's modulus, Poisson ratio and density of 375 GPa, 0.3, and 4370 kg/m^3, respectively, while Co-Cr-Mo metal alloy couple has a Young's modulus 210 GPa, Poisson's ratio 0.3 and density 8000 kg/m^3. The wear factor for CoC and MoM couples was considered to be equal to 0.2×10^{-8} and 0.5×10^{-8} mm^3/Nm^{-1}, respectively [10]. Three-dimensional physiological forces

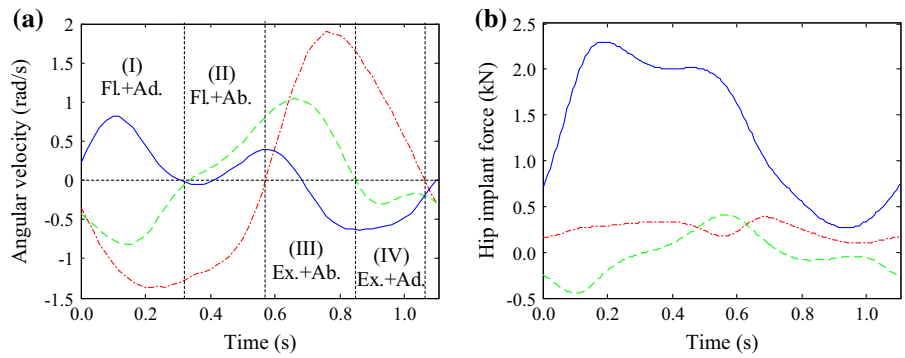

Fig. 10 (a) Angular velocities where *solid line* ω_z(IER); *dashed lines* ω_y(AA); *dash-dotted lines* ω_x(FE); (b) physiological adopted forces with *solid line* f_z(vertical); *dashed lines* f_y(A-P); *dash-dotted lines* f_x(M-L) for the gait cycle [34]

and angular velocities were extracted from the literature, which are plotted in the diagrams of Fig. 10 [34]. According to the presented approach, the cup and femoral head surfaces were discretized into several elements and the accuracy and convergence of results were assessed by varying the parameter $\varkappa$, as it can be observed in Table 1. A value for the parameter $\varkappa$ equal to 360 ensures both accuracy and convergence of the simulation. Hence, the number of elements for this study was 129,600 on the cup surface and 259,200 on the head surface. In order to assess if very small size elements affected the results, $\varkappa = 900$ was also considered, in which the number of elements within the cup surface was 810,000 and the head surface 1,620,000. This assessment showed that outcomes did not vary with this very small element size. Furthermore, the two-step and three-step Adams–Bashforth method were considered to check the accuracy of numerical integrations for wear depth calculated from the Euler integration algorithm, Eq. (23). A very good agreement was observed among results obtained from those methods.

Table 1 The convergence and accuracy assessment with varying $\varkappa$

$\varkappa$	Head linear wear rate (mm/year)	Head linear wear rate (mm/year)	Volumetric wear rate (mm^3/year)
45	0.170	0.093	6.932
90	0.172	0.094	6.932
180	0.173	0.095	6.932
360	0.173	0.095	6.932
540	0.173	0.095	6.932
720	0.173	0.095	6.932
900	0.173	0.095	6.932

6.1 Silent hips or very low friction hip implants

With the purpose to validate the reliability of the developed approach, linear and volumetric wear rates computed for one million cycles have been evaluated for the aforementioned material and geometry properties of ceramic-on-ceramic hip arthroplasties subject to physiological angular motions and forces. It was demonstrated that the linear wear rate evaluated using the proposed approach, 1.87 μm/year, is in agreement with clinical data [66–68]. In turn, the volumetric wear rate was evaluated with the presented model, which is equal to 0.14 mm^3/year, is relatively close to finite element outcome [10] and hip simulator reports [68,69]. Moreover, a retrieval study conducted by Walter et al. [70] showed silent hips experience 0.14 mm^3/year, which strongly corroborates with the results reported here.

In addition, the wear of MoM hip implant has also been studied by considering the proposed approach. Thus, the linear and volumetric wear rates produced were equal to 2.34 μm/year and 0.22 mm^3/year, respectively, which are in line with those available in the best-published literature [10,11,71] and hip simulators [72,73].

Another comparison that allows for the validation of the proposed approach carried out against a recent investigation with similar geometric and material properties and angular motion and forces with the clearance 30 μm. Results were obtained for a hip with frictionless contact as mentioned in reference [11]. A frictionless contact reflects the idea that the simulation neglects the effect of friction on the contact pressure and contact point trajectory in the hip prosthesis. However, the effect of friction is included into the wear factor to predict wear. Thus, the results produced with the pre-

sented methodology shows a maximum deviation of 3.5 % when compared with data available in Ref. [11]. Furthermore, the maximum linear wear of the femoral head and cup was 2.86 and 1.89 μm/year, respectively, and the total volumetric wear was 0.21 mm^3/year.

6.2 Noisy hips or high friction contact hip implants

It has been recognized that only a few wear models available in the literature account for the effect of friction phenomenon on contact stress and the trajectory of contact point [10,11]. Some of them simply neglect the influence of friction by considering frictionless contacts [74,75]. The femoral head has a relative sliding against the cup over the gait cycle in vivo. It is known that when two surfaces slide against each other, friction develops and acts as a resistance to relative motion [31]. Moreover, friction can induce vibration in the trajectory of the contact point between the head and cup owing to stick-slip, mode-coupling and negative damping in the system [29,31]. In this regard, friction-induced vibration has been also reported as a potential cause of hip squeaking in ceramic-on-ceramic hip implants [29,76]. Consequently, friction can affect the sliding distance and contact stress which are important parameters influencing wear. Mattei and Di Puccio [11] investigated the influence of friction on the trajectory of the contact point in MoM hip implants, being reported that linear wear rates for high friction hips are less than that of frictionless case. However, one retrieval investigation concluded that noisy CoC hip arthroplasties represented a 45-fold increase in their wear compared to silent hips [70]. It is worth noting that the previous computational studies taking friction effect into account did not include one of the main consequences of friction in artificial hip joint which is friction-induced vibration causing CoC hip prostheses to squeak. It has been reported that the femoral head vibrates inside the cup on top of the normal gross motion with micron amplitude in the collision plane due to friction-induced vibration [29,31]. Moreover, the contact point trajectory onto the cup surface showed an oscillatory behavior due to friction-induced vibration and physiological motions and forces [31]. Based on Archard's wear model, any modification in the shape of the contact point track significantly affects wear prediction [22]. Additionally, it was illustrated that friction can import an oscillatory behavior into the contact pressure at the contact point which ultimately affects the wear prediction [30]. To the best of the authors' knowledge, the problem of the friction-induced vibration on the wear prediction has not been yet mentioned in the literature.

Considering the influence of friction-induced vibration on ceramic-on-ceramic hip implants, the present investigation showed that volumetric wear rates of noisy hips due to friction-induced vibration is 6.9 mm^3/year, which is consistent with the retrieval outcome, 6.7 mm^3/year, reported by Walter et al. [70]. In turn, the linear wear rates of the cup and head are 0.095 and 0.173 mm/year, respectively, which are corroborated by clinical data [68]. It must be highlighted that the linear wear rate on the cup surface reported by Walter et al. [70] was 0.093 mm/year (mean of 60 and 125 μm/year) for the head radius 14 mm, which conforms to our prediction.

6.3 Contact point trajectory and wear map

In this section, the contact point trajectories onto the femoral head and cup are investigated. With the purpose to compare the trajectory shapes, they are projected onto the plane inclined from the horizontal plane with an angle of $\pi/4$. As can be observed in Fig. 11, the contact point track has different shapes on the cup and head surfaces. This happens since the cup is stationary, while the femoral head freely moves due to the physiological motions. The effect of friction on the sliding track is illustrated in Fig. 11, in which Fig. 11a depicts the trajectory of low friction hip implant articulation and Fig. 11d the trajectory with high friction. The contact point trajectories of the femoral head and cup over the gait cycle having a loop shape widen as friction increases. The effect of friction-induced vibration on the trajectories is clearly visible by a comparison between the low friction and high friction trajectories of the femoral head and cup. From the analysis of Fig. 11, it can be observed that the head and cup trajectories for high friction case are much thicker than that of low friction articulation. These thick lines show the oscillatory behavior of contact point trajectory.

Furthermore, wear map onto the cup and head surfaces is shown in Fig. 11 for both low and high friction mechanisms. As can be seen, the wear maps conform to the corresponding trajectories of the cup and head in terms of location and shape. The dark red color in the wear map illustrates the area where the maximum

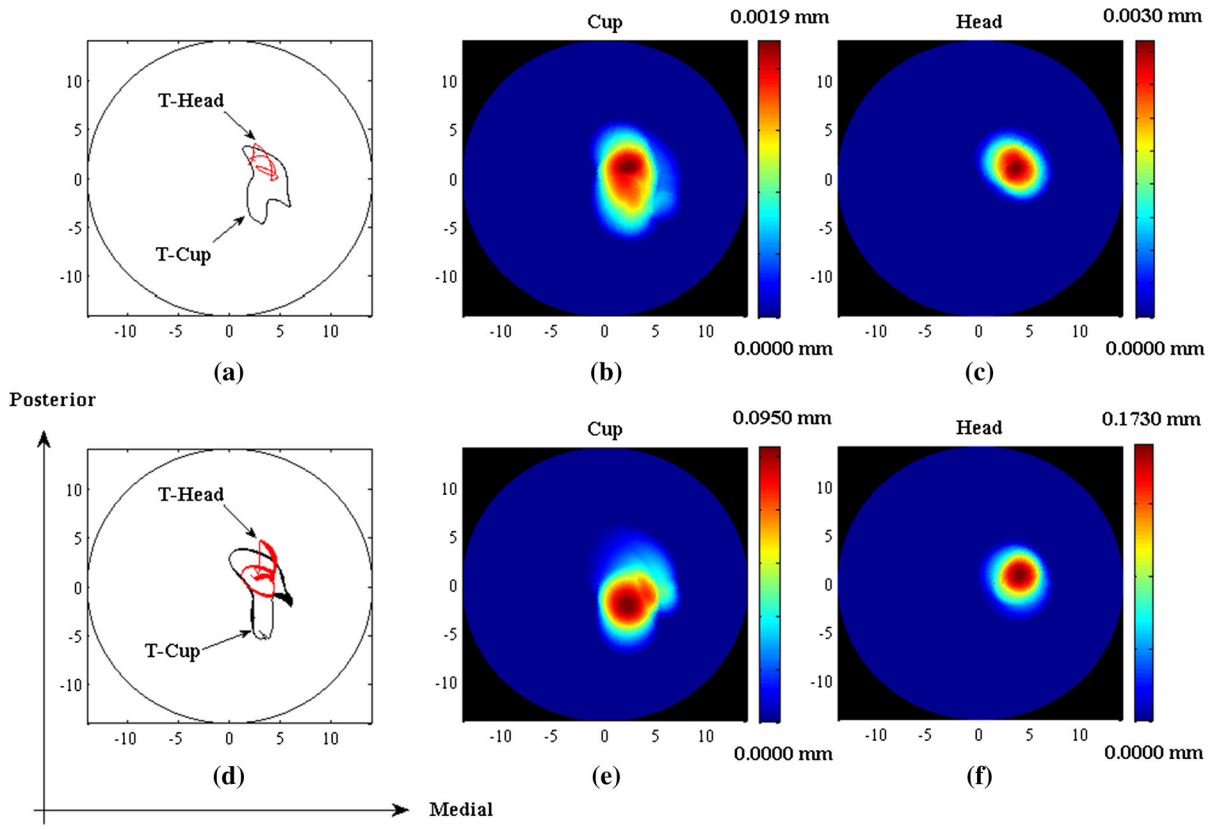

Fig. 11 Ceramic-on-ceramic (CoC) hip implant with three-dimensional physiological loading and motion of the human body with very low friction, $c_f/c_d = 0.0001/0.000065$ where volumetric wear is equal to 0.14 mm^3 (top row) and high friction where volumetric wear is equal to 6.9 mm^3 and $c_f/c_d = 0.1/0.065$ (bottom row): (**a**) and (**d**) contact point trajectory on the head and cup, illustrated as T-Head and T-Cup, respectively; (**b**) and (**e**) linear wear depth on the cup; (**c**) and (**f**) linear wear depth on the head

linear material loss takes place. The wear map of the cup is different with the femoral head for both low and high friction systems. Increasing friction resulted in a shift of the location of the contact area which can thus change the cup wear map location and shape. In addition, maximum linear wear on the head is more than that on the cup surface since the contact point track of the cup is wider than that of the femoral head. It is worth noting that volumetric wear rates of the high friction hip arthroplasty are around 49 times greater than very low friction system. It can prove the significant effect of friction on wear prediction.

Regarding the determination of maximum linear wear within the cup surface, it is worth to discuss hip implant fracture as an important issue with ceramic-on-ceramic hip implants. Alumina ceramic bearings are one of the most promising artificial hip joints due to their biocompatibility, high hardness, perfect chemical inertia and low coefficient of friction. However, the brittleness of alumina ceramic components is a drawback with CoC hip implants, which may lead to fracture. The cause of the fracture is propagation of cracks due to the stress concentration. When cyclic loads are applied over the ceramic components due to both million cycles of body movement and oscillation owing to friction, microscopic imperfections such as pores or inhomogeneity of the material can act as stress risers leading to the propagation of cracks with potential component failure. As illustrated, the present study can address the maximum linear wear and corresponding location within the cup surface. From a mechanical point of view, the cup experiences the maximum stress concentration in proximity of the location with the smallest thickness, which is most likely to fail due

Table 2 The effect of hip implant size on predicted wear rates

Hip diameter (mm)	Head linear wear rate (mm/year)	Cup linear wear rate (mm/year)	Volumetric wear rate (mm^3/year)
28	0.17	0.10	6.9
32	0.19	0.10	9.6
36	0.21	0.11	12.7
40	0.22	0.12	16.1

Table 3 The effect of hip implant clearance on predicted wear rates, hip diameter: 28mm

Clearance (μm)	Head linear wear rate (mm/year)	Cup linear wear rate (mm/year)	Volumetric wear rate (mm^3/year)
10	0.25	0.21	26.5
30	0.19	0.12	10.5
50	0.17	0.10	6.9
70	0.16	0.09	5.3
90	0.15	0.08	4.4

to the fracture. Therefore, the present model can advise the location of potential fracture in the acetabular cup. Moreover, the fracture direction may be determined using the direction of contact point trajectory at the area with the maximum linear wear.

6.4 Hip implant size and clearance and the Stribeck friction model

The effect of hip prosthesis size and clearance on linear and volumetric wear rates is visible in the values listed in Tables 2 and 3. As can be observed in Table 2 that hip component wear increases with the size of the hip implant. Hence, it causes the trajectory of the contact point to widen giving rise to the sliding distance influencing wear prediction. In addition, hip implant size affects mostly volumetric wear rates and slightly changes linear wear rates. In contrast, decreasing wear rates is a result of increasing hip implant clearance, that is, the greater the clearance, the less the predicted wear rates. In this case, as clearance size decreases, maximum contact pressure decreases and contact area increases [30]. This observation is particularly important since the wear depends on both contact pressure and sliding distance regarding the Archard's wear model. Therefore, the sliding distance should increase such that an increase in wear rates is obtained, although contact pressure decreases.

Table 4 The effect of Stribeck friction model parameters on predicted wear rates, hip diameter: 28mm

ξ	v_0	$c_{f/}\, c_d$	Volumetric wear rate (mm^3/year)
5	0.01	0.1/0.065	6.0
10	0.01	0.1/0.065	6.9
15	0.01	0.1/0.065	8.2
10	0.005	0.1/0.065	10.32
10	0.02	0.1/0.065	1.3
10	0.01	0.05/0.0325	5.8
10	0.01	0.2/1.3	9.33

Table 4 presented the influence of friction model parameters on volumetric wear of hip implant. As observed, an increase in ξ leads to an increase in wear volume. ξ appears in the second equation in (21) representing the Stribeck friction effect and affecting friction-induced vibration. It may affect the trajectory of contact point, which leads to a variation of volumetric wear. v_0 has a very interesting influence on wear prediction as seen in Table 4. When it becomes smaller, the dynamic system experiences more the stick-slip and Stribeck effect leading to greater friction-induced vibration, which consequently increases predicted wear volume. In contrast, when it is 0.02, the predicted wear is sharply decreased. It may occur because the relative velocity of system is mostly less than 0.02 and the system does not vibrate due to stick-slip and negative slope effect. Increasing $c_{f/}c_d$ increases volumetric wear as physically expected.

Moreover, Fig. 12 depicted the Stribeck and stick-slip effect on the dynamic response of the system over a gait cycle. When the relative tangential speed between the femoral head and cup at the contact point is very low, stick-slip phenomenon arises because of the difference between static and kinetic friction. Moreover, the Stribeck model captures negative slop effect of friction which leads to friction-induced vibration by introducing a negative damping component in the equations of motion. The plot can be categorized by three phases, namely stick, stick-slip and pure slip. In the quasi-static stick phase, friction lies on the very steep, negative-sloping region of the friction curve. The femoral head

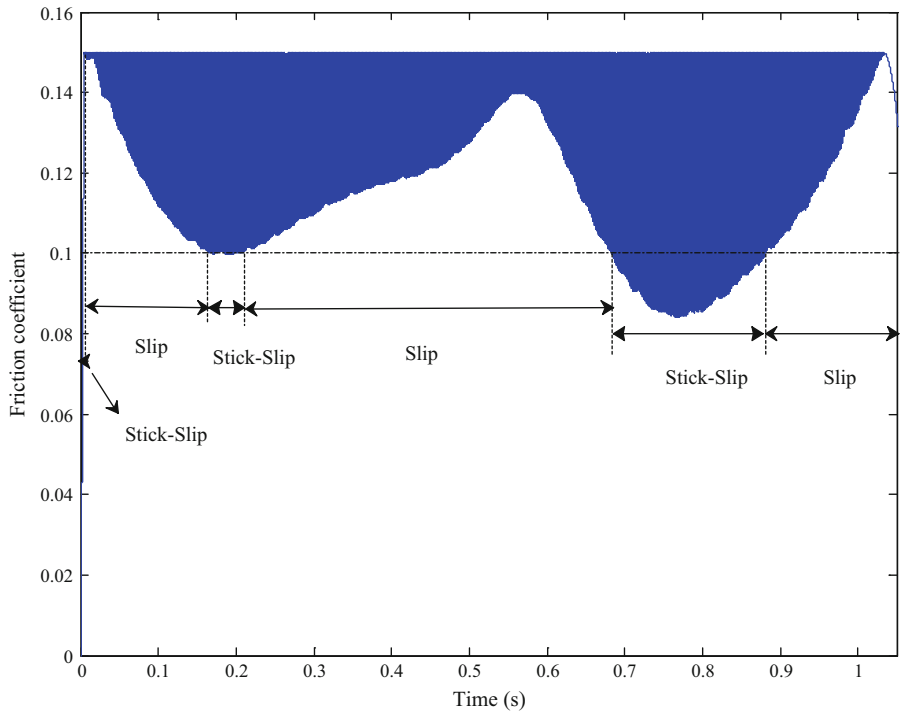

Fig. 12 The Stribeck and stick-slip phenomena over one normal walking cycle

goes from stick to slip and vice versa repeatedly in the stick-slip region. During the slip part, friction decreases as the velocity increases owing to negative-sloping velocity.

6.5 High wear rates

Hip simulator and computational studies on CoC and MoM bearings have consistently shown very low wear rates under standard hip simulator conditions, which correlates with well-positioned prostheses [10,77]. However, this has not been confirmed by long-term retrieval analyses [78–80]. The standard conditions are defined as the inclination angle of the acetabular cup is below a clinical equivalent of 55°, and the femoral head and the cup are concentric. Under such conditions, the contact area occurs within the intended bearing surface and very low wear rates have been obtained. Conversely, CoC and MoM retrievals with high wear rates have been associated with steep cup inclination angle resulting in edge loading [81,82]. Increased cup inclination angle has been associated with a stripe wear area on the femoral head and an elevated wear rate of alumina ceramic-on-ceramic retrievals [83]. However, the steep cup inclination angle in vitro studies do not lead to high wear levels observed in in vivo and even the corresponding wear mechanisms [81,82].

Introducing microseparation to the gait cycle was shown that microseparation resulted in edge loading, wear rates and wear mechanisms similar to those retrieved hip prostheses with high wear rates [84,85]. The loading and motion inputs affect hip implant wear. Fialho et al. [86] showed that the wear rates occurred during the jogging cycle showed a twofold increase compared to those of the walking cycle, due to a very significant increase in loading. Considering the effect of different motion inputs on wear prediction of hip prostheses, it is indicated that evaluated volumetric wear under the ProSim simulator and the ISO motion and loading conditions are less than that computed from one subject to in vivo walking motion [87].

Friction can affect sliding distance and contact stress in artificial hip joints [11,31]. It was reported that the femoral head vibrates inside the cup with micron amplitude within the corresponding collision plane and with nanometer amplitude normal to the collision plane due to friction-induced vibration [29,31]. This results in a change in the contact point trajectory in both micro- and macroscales as well as in contact stress. Based on Archard's wear model, any alteration in the shape of the contact point track significantly affects wear prediction

[22]. The present study hypothesized that high friction may cause excessive wear rates onto the femoral head and cup articulation. From the obtained results, it has been illustrated that friction-induced vibration significantly increases wear in artificial hip joints. Hence, friction-induced vibration may be one of the main causes of excessive wear observed in vivo.

Friction coefficient at the bearing interface depends on bearing materials, lubricant, bearing clearances, surface roughness and the gait motion and loads [10,88]. The coefficient of friction in CoC hip devices reported in available literature is in the range of 0.04–0.13 [88–90]. The broad range of friction factor is due to measuring friction coefficient with different lubricants, different bearing loads, the presence of particulate debris, malposition of prosthesis components and different instances of the gait motion. The wear coefficient depends on coupled materials, interfacial friction, the geometry of contacting surfaces, the coupled material wettability and lubrication [2,88]. It has been obtained either from hip simulator or from pin-on-disk tests [73,91]. Moreover, there are significant technical challenges with properly modeling the dynamics of articulating components along with the presence of fluid-film lubrication and in vivo conditions.

7 Concluding remarks

The effect of friction-induced vibration on predicted wear rates in hard hip replacements has been investigated throughout this work. For this, a multibody dynamic approach was developed to integrate the Archard's wear model into the dynamic formulation in order to predict linear and volumetric wear of artificial hip joints. The gross movement and vibration of the femoral head inside the cup for both low and high frictional contacts were modeled and wear evaluated. The modification of hip implant couple geometries was also taken into account by updating the corresponding surface geometries as the simulation progressed. The proposed approach demonstrated promising results in comparison with the available literature from different sources such as other computational results, hip simulator reports and clinical data.

The present study showed that the contact point trajectory onto the cup surface was different from that onto the femoral head surface. Moreover, it was illustrated that friction had a significant effect on the contact point trajectory in both micro- and macroscale. It widened the loop shape of the contact point trajectory and induced vibration in the femoral head motion onto the cup surface. The later was observed in the plots as a thick trajectory curve and increased sliding distance. Moreover, the wear maps were depicted, which showed the wear distribution onto the femoral head and cup surfaces. They conformed to the contact point path onto both the acetabular cup and head in terms of location and shape and their shape and location changed as friction increased. The effect of hip implant size and clearance on wear prediction were also considered and analyzed.

An important achievement of the present investigation was to show computationally that friction-induced vibration significantly increases predicted wear rates in ceramic-on-ceramic hip prostheses. In fact, it was demonstrated that noisy CoC hip implants represent a 49-fold increase in predicted wear rates with respect to silent hips. The hypothesis that friction-induced vibration may be one of the main causes of the high wear rates, observed clinically, was corroborated in the present work.

Acknowledgments The first author gratefully acknowledges Macquarie University for his International Macquarie University Research Excellence Scholarship (iMQRES)—No. 2010017. The second author would like to thank the Portuguese Foundation for Science and Technology (FCT) through the project UID/EEA/04436/2013.

References

1. Ibrahim, R.A.: Friction-induced vibration, chatter, squeal, and chaos. Part I: mechanics of contact and friction. Appl. Mech. Rev. **47**(7), 209–226 (1994)
2. Teoh, S.H., Chan, W.H., Thampuran, R.: An elasto-plastic finite element model for polyethylene wear in total hip arthroplasty. J. Biomech. **35**(3), 323–330 (2002)
3. Sfantos, G.K., Aliabadi, M.H.: Total hip arthroplasty wear simulation using the boundary element method. J. Biomech. **40**, 378–389 (2007)
4. Jourdan, F., Samida, A.: An implicit numerical method for wear modelling applied to a hip joint prosthesis problem. Comput. Methods Appl. Mech. Eng. **198**, 2209–2217 (2009)
5. Bevill, S.L., Bevill, G.R., Penmetsa, J.R., Petrella, A.J., Rullkoetter, P.J.: Finite element simulation of early creep and wear in total hip arthroplasty. J. Biomech. **38**, 2365–2375 (2005)
6. Kang, L., Galvin, A.L., Fisher, J., Jin, Z.: Enhanced computational prediction of polyethylene wear in hip joints by incorporating cross-shear and contact pressure in addition

to load and sliding distance: effect of head diameter. J. Biomech. **42**, 912–918 (2009)
7. Matsoukas, G., Willing, R., Kim, Y.: Total hip wear assessment: a comparison between computational and in vitro wear assessment techniques using ISO14242 loading and kinematics. J. Biomech. Eng. **131**, 1–11 (2009)
8. Mattei, L., Di Puccio, F., Ciulli, E.: A comparative study of wear laws for soft-on-hard hip implants using a mathematical wear model. Tribol. Int. **63**, 66–77 (2013)
9. Liu, F., Leslie, I., Williams, S., Fisher, J., Jin, Z.: Development of computational wear simulation of metal-on-metal hip resurfacing replacements. J. Biomech. **41**, 686–694 (2008)
10. Uddin, M.S., Zhang, L.C.: Predicting the wear of hard-on-hard hip joint prostheses. Wear **301**, 192–200 (2013)
11. Mattei, L., Di Puccio, F.: Wear simulation of metal-on-metal hip replacements with frictional contact. J. Tribol. **135**(2), 021402, 12p (2013)
12. Dowson, D., Jin, Z.: Metal-on-metal hip joint tribology. Proc. Inst. Mech. Eng. H J. Eng. Med. **220**, 107–118 (2006)
13. Essner, A., Sutton, K., Wang, A.: Hip simulator wear comparison of metal-on-metal, ceramic-on-ceramic and cross-linked UHMWPE bearings. Wear **259**, 992–995 (2005)
14. Flores, P.: Modeling and simulation of wear in revolute clearance joints in multibody systems. Mech. Mach. Theory **44**, 1211–1222 (2009)
15. Meng, H.C., Ludema, K.C.: Wear models and predictive equations: their form and content. Wear **181–183**, 443–457 (1995)
16. Mukras, S., Kim, N.H., Sawyer, W.G., Jackson, D.B., Bergquist, L.W.: Numerical integration schemes and parallel computation for wear prediction using finite element method. Wear **266**, 822–831 (2009)
17. Su, Y., Chen, W., Tong, Y., Xie, Y.: Wear prediction of clearance joint by integrating multi-body kinematics with finite-element method. Proc. Inst. Mech. Eng. J J. Eng. Tribol. **1**(224), 815–823 (2010)
18. Quental, C., Folgado, J., Ambrósio, J., Monteiro, J.: A multibody biomechanical model of the upper limb including the shoulder girdle. Multibody Syst. Dyn. **28**(1–2), 83–108 (2012)
19. Hegadekatte, V., Huber, N., Kraft, O.: Finite element based simulation of dry sliding wear. Model. Simul. Mater. Sci. Eng. **13**, 57–75 (2005)
20. Flodin, A., Andersson, S.: A simplified model for wear prediction in helical gears. Wear **249**, 285–292 (2001)
21. Raimondi, M.T., Santambrogio, C., Pietrabissa, R., Raffelini, F., Molfetta, L.: Improved mathematical model of the wear of the cup articular surface in hip joint prostheses and comparison with retrieved components. Proc. Inst. Mech. Eng. H J. Eng. Med. **215**(4), 377–391 (2001)
22. Archard, J.F.: Contact and rubbing of flat surfaces. J. Appl. Phys. **24**, 981–988 (1953)
23. Barbour, P.S.M., Stone, M.H., Fisher, J.: A hip joint simulator study using simplified loading and motion cycles generating physiological wear paths and rates. Proc. Inst. Mech. Eng. H J. Eng. Med. **213**(6), 455–467 (1999)
24. Saikko, V., Calonius, O., Kernen, J.: Effect of slide track shape on the wear of ultra-high molecular weight polyethylene in a pin-on-disk wear simulation of total hip prosthesis. J. Biomed. Mater. Res. B Appl. Biomater. **69B**(2), 141–148 (2004)
25. Ramamurti, B., Bragdon, C.R., O'Connor, D.O., Lowenstein, J.D., Jasty, M., Estok, D.M., Harris, W.H.: Loci of movement of selected points on the femoral head during normal gait: three-dimensional computer simulation. J. Arthoplasty **11**(7), 845–852 (1996)
26. Saikko, V., Calonius, O.: Slide track analysis of the relative motion between femoral head and acetabular cup in walking and hip simulator. J. Biomech. **35**(4), 455–464 (2002)
27. Sariali, E., Stewart, T., Jin, Z., Fisher, J.: Three-dimensional modelling of in vitro hip kinematics under micro-separation regime for ceramic on ceramic total hip prosthesis: an analysis of vibration and noise. J. Biomech. **43**, 326–333 (2010)
28. Sawyer, W.G.: Wear predictions for a simple-cam including the coupled evolution of wear and load. J. Soc. Tribol. Lubr. Eng. **57**, 31–36 (2001)
29. Weiss, C., Hothan, A., Huber, G., Morlock, M., Hoffmann, N.: Friction-induced whirl vibration: root cause of squeaking in total hip arthroplasty. J. Biomech. **45**, 297–303 (2012)
30. Askari, E., Flores, P., Dabirrahmani, D., Appleyard, R.: Study of the friction-induced vibration and contact mechanics of artificial hip joints. Tribol. Int. **70**, 1–10 (2014)
31. Askari, E., Flores, P., Dabirrahmani, D., Appleyard, R.: Nonlinear vibration and dynamics of ceramic on ceramic artificial hip joints: a spatial multibody modelling. Nonlinear Dyn. **76**, 1365–1377 (2014)
32. Nikravesh, P.E.: Computer-Aided Analysis of Mechanical Systems. Prentice Hall, Englewood Cliffs (1988)
33. Machado, M., Moreira, P., Flores, P., Lankarani, H.M.: Compliant contact force models in multibody dynamics: evolution of the Hertz contact theory. Mech. Mach. Theory **53**, 99–121 (2012)
34. Bergmann, G., Deuretzbacher, G., Heller, M., Graichen, F., Rohlmann, A., Strauss, J., Duda, G.N.: Hip contact forces and gait patterns from routine activities. J. Biomech. **34**(7), 859–871 (2001)
35. Ribeiro, A., Rasmussen, J., Flores, P., Silva, L.F.: Modeling of the condyle elements within a biomechanical knee model. Multibody Syst. Dyn. **28**, 181–197 (2012)
36. Lopes, P.S.T.: Geometric and structural analysis of the locking mechanism between liner and acetabular cup. MSc Dissertation in Biomedical Engineering, University of Minho, Guimarães, Portugal (2007)
37. Stops, A., Wilcox, R., Jin, Z.: Computational modelling of the natural hip: a review of finite element and multibody simulations. Comput. Methods Biomech. Biomed. Eng. **15**(9), 963–979 (2012)
38. Mattei, L., Di Puccio, F., Piccigallo, B., Ciulli, E.: Lubrication and wear modeling of artificial hip joints: a review. Tribol. Int. **44**, 532–549 (2011)
39. Blajer, W., Czaplicki, A., Dziewiecki, K., Mazur, Z.: Influence of selected modeling and computational issues on muscle force estimates. Multibody Syst. Dyn. **24**, 473–492 (2010)
40. Ambrosio, J.: Rigid and flexible multibody dynamics tools for the simulation of systems subjected to con-tact and impact conditions. Eur. J. Solids A/Solids **19**, S23–44 (2000)
41. Cappozzo, A., Gazzani, F.: Joint kinematic assessment during physical exercise. In: Berme, N., Cappozzo, A. (eds.) Biomechanics of Human Movement: Applications in Reha-

bilitation, Sports and Ergonomics, pp. 263–274. Bertec Corp., Worthington, Ohio (1990)
42. Flores, P., Lankarani, H.M.: Dynamic response of multibody systems with multiple clearance joints. ASME J. Comput. Nonlinear Dyn. **7**(3), 031003, 13p (2012)
43. Flores, P., Lankarani, H.M.: Spatial rigid-multibody systems with lubricated spherical clearance joints: modeling and simulation. Nonlinear Dyn. **60**, 99–114 (2010)
44. Flores, P., Machado, M., Silva, M.T., Martins, J.M.: On the continuous contact force models for soft materials in multibody dynamics. Multibody Syst. Dyn. **25**(3), 357–375 (2011)
45. Quental, C., Folgado, J., Ambrásio, J., Monteiro, J.: Critical analysis of musculoskeletal modelling complexity in multibody biomechanical models of the upper limb. Comput. Method Biomech. Biomed. Eng. **18**(7), 749–759 (2015)
46. Flores, P., Ambrosio, J., Claro, J.C.P., Lankarani, H.M.: Dynamics of multibody systems with spherical clearance joints. J. Comput. Nonlinear Dyn. **1**, 240–247 (2006)
47. Tian, Q., Zhang, Y., Chen, L., Flores, P.: Dynamics of spatial flexible multibody systems with clearance and lubricated spherical joints. Comput. Struct. **87**(13–14), 913–929 (2009)
48. Ahmed, S., Lankarani, H.M., Pereira, M.F.O.S.: Frictional impact analysis in open loop multibody mechanical system. J. Mech. Des. **121**, 119–127 (1999)
49. Flores, P., Ambrósio, J.: On the contact detection for contact-impact analysis in multibody systems. Multibody Syst. Dyn. **24**(1), 103–122 (2010)
50. Flores, P., Ambrósio, J., Claro, J.C.P., Lankarani, H.M.: Spatial revolute joints with clearance for dynamic analysis of multibody systems. Proc. Inst. Mech. Eng. K J. Multi-body Dyn. **220**(4), 257–271 (2006)
51. Silva, P., Silva, M.T., Martins, J.: Evaluation of the contact forces developed in the lower limb/orthosis interface for comfort design. Multibody Syst. Dyn. **24**, 367–388 (2010)
52. Lopes, D.S., Silva, M.T., Ambrósio, J.A., Flores, P.: A mathematical framework for contact detection between quadric and superquadric surfaces. Multibody Syst. Dyn. **24**(3), 255–280 (2010)
53. Machado, M., Flores, P., Ambrósio, J., Completo, A.: Influence of the contact model on the dynamic response of the human knee joint. Proc. Inst. Mech. Eng. K J. Multi-body Dyn. **225**(4), 344–358 (2011)
54. Flores, P., Leine, R., Glocker, C.: Application of the non-smooth dynamics approach to model and analysis of the contact-impact events in cam-follower systems. Nonlinear Dyn. **69**, 2117–2133 (2012)
55. Koshy, C.S., Flores, P., Lankarani, H.M.: Study of the effect of contact force model on the dynamic response of mechanical systems with dry clearance joints: computational and experimental approaches. Nonlinear Dyn. **73**(1–2), 325–338 (2013)
56. Hairer, E., Nørsett, S., Wanner, G.: Solving Ordinary Differential Equations I: Nonstiff Problems, 2nd edn. Springer, Berlin (1993)
57. Lankarani, H.M., Nikravesh, P.E.: A contact force model with hysteresis damping for impact analysis of multibody systems. J. Mech. Des. **112**, 369–376 (1990)
58. Love, A.E.H.: A Treatise on the Mathematical Theory of Elasticity, 4th edn. Dover Publications, New York (1944)
59. Goldsmith, W.: Impact. The Theory and Physical Behaviour of Colliding Solids. Edward Arnold Ltd, London (1960)
60. Machado, M., Flores, P., Claro, J.C.P., Ambrósio, J., Silva, M., Completo, A., Lankarani, H.M.: Development of a planar multi-body model of the human knee joint. Nonlinear Dyn. **60**, 459–478 (2010)
61. Hetzler, H., Schwarzer, D., Seemann, W.: Analytical investigation of steady-state stability and Hopf-bifurcations occurring in sliding friction oscillators with application to low-frequency disc brake noise. Commun. Nonlinear Sci. Numer. Simul. **12**, 83–99 (2007)
62. Kanga, J., Krousgrilla, C.M., Sadeghi, F.: Oscillation pattern of stick-slip vibrations. Int. J. Non-Linear Mech. **44**, 820–828 (2009)
63. Bengisu, M.T., Akay, A.: Stability of friction-induced vibrations in multi-degree-of-freedom systems. J. Sound Vib. **171**, 557–570 (1994)
64. Hertz, H.: Über die Berührung fester elastischer Körper. J. Reine Angew. Math. **92**, 156–171 (1881)
65. Craig, J.J.: Introduction to Robotics: Mechanics and Control, 2nd edn. Addison-Wesley Longman, Reading (1989)
66. Dorlot, J.M.: Long-term effects of alumina components in total hip prostheses. Clin. Orthop. Rel. Res. **282**, 47–52 (1992)
67. Mittelmeier, H., Heisel, J.: Sixteen years' experience with ceramic hip pros-theses. Clin. Orthop. Rel. Res. **282**, 64–72 (1992)
68. Affatato, S., Traina, F., De Fine, M., Carmignato, S., Toni, A.: Alumina-on-alumina hip implants: a wear study of retrieved components. J. Bone Joint Surg. **94–B**, 37–42 (2012)
69. Stewart, T., Nevelos, J., Tipper, J., Insley, G., Streicher, R., Ingham, E., Fisher, J.: Long term simulator studies of alumina ceramic/ceramic hip joints with swing phase micro-separation; analysis of wear and wear debris generation. In: Combined Orthopaedic Research Societies Meeting, Rhodes, Greece (2001)
70. Walter, W.L., Kurtz, S.M., Esposito, C., Hozack, W., Holley, K.G., Garino, J.P., Tuke, M.A.: Retrieval analysis of squeaking alumina ceramic-on-ceramic bearings. J. Bone Joint Surg. **93–B**(2), 1597–1601 (2011)
71. Harun, M.N., Wang, F.C., Jin, Z.M., Fisher, J.: Long-term contact-coupled wear prediction for metal-on-metal total hip joint replacement. J. Eng. Tribol. **223**, 993–1001 (2009)
72. Medley, J.B., Chan, F.W., Krygier, J.J., Bobyn, J.D.: Comparison of alloys and designs in a hip simulator study of metal on metal implants. Clin. Orthop. Rel. Res. **329**, 148–149 (1996)
73. Chan, F.W., Bobyn, J.D., Medley, J.B., Krygier, J.J., Tanzer, M.: The Otto Aufranc Award. Wear and lubrication of metal-on-metal hip implants. Clin. Orthop. Rel. Res. **369**, 10–24 (1999)
74. Liu, F., Jin, Z.M., Grigoris, P., Hirt, F., Rieker, C.: Contact mechanics of metal-on-metal hip implants employing a metallic cup with a Uhmwpe backing. Proc. Inst. Mech. Eng. H J. Eng. Med. **217**(3), 207–213 (2003)
75. Udofia, I.J., Yew, A., Jin, Z.M.: Contact mechanics analysis of metal-on-metal hip resurfacing prostheses. Proc. Inst. Mech. Eng. H J. Eng. Med. **218**(5), 293–305 (2004)

76. Askari, E., Flores, P., Dabirrahmani, D., Appleyard, R.: A computational analysis of squeaking hip prostheses. ASME J. Comput. Nonlinear Dyn. **10**(2) (2015)
77. Goldsmith, A.A., Dowson, D., Isaac, G.H., Lancaster, J.G.: A comparative joint simulator study of the wear of metal-on-metal and alternative material combinations in hip replacements. Proc. Inst. Mech. Eng. H J. Eng. Med. **214**(1), 39–47 (2000)
78. Sieber, H.P., Rieker, C.B., Kottig, P.: Analysis of 118 Second-generation metal-on-metal retrieved hip implants. J. Bone Joint Surg. **81–B**(1), 46–50 (1999)
79. Affatato, S., Taddei, P., Carmignato, S., Modena, E., Toni, A.: Severe damage of alumina-on-alumina hip implants: wear assessments at a microscopic level. J. Eur. Ceram. Soc. **32**(14), 3647–3657 (2012)
80. Reinisch, G., Judmann, K.P., Lhotka, C., Lintner, F., Zweymuller, K.A.: Retrieval study of un-cemented metal-on-metal hip prostheses revised for early loosening. Biomaterials **24**(6), 1081–1091 (2003)
81. Al-Hajjar, M., Fisher, J., Tipper, J.L., Williams, S., Jennings, L.M.: Wear of 36-mm BIOLOX(R) delta ceramic-on-ceramic bearing in total hip replacements under edge loading conditions. Proc. Inst. Mech. Eng. H J. Eng. Med. **227**(5), 535–542 (2013)
82. Fisher, J., Al-Hajjar, M., Williams, S., Tipper, J., Ingham, E., Jennings, L.: Simulation and measurement of wear in metal-on-metal bearings in vitro-understanding the reasons for increased wear. Orthop. Trauma **26**(4), 253–258 (2012)
83. Nevelos, J.E., Ingham, E., Doyle, C., Nevelos, A.B., Fisher, J.: The influence of acetabular cup angle on the wear of "BIOLOX Forte" alumina ceramic bearing couples in a hip joint simulator. J. Mater. Sci. Mater. Med. **12**, 141–144 (2001)
84. Hatton, A., Nevelos, J.E., Nevelos, A.A., Banks, R.E., Fisher, J., Ingham, E.: Alumina-alumina artificial hip joints. Part I: a histological analysis and characterisation of wear debris by laser capture microdissection of tissues retrieved at revision. Biomaterials **23**(16), 3429–3440 (2002)
85. Al-Hajjar, M., Jennings, L.M., Begand, S., Oberbach, T., Delfosse, D., Fisher, J.: Wear of novel ceramic-on-ceramic bearings under adverse and clinically relevant hip simulator conditions. J. Biomed. Mater. Res. B Appl. Biomater. **101**(8), 1456–1462 (2013)
86. Fialho, J.C., Fernandes, P.R., Eca, L., Folgado, J.: Computational hip joint simulator for wear and heat generation. J. Biomech. **40**(11), 2358–2366 (2007)
87. Liu, F., Fisher, J., Jin, Z.M.: Effect of motion inputs on the wear prediction of artificial hip joints. Tribol. Int. **63**, 105–114 (2013)
88. Scholes, S.C., Unsworth, A., Goldsmith, A.A.J.: A frictional study of total hip joint replacements. Phys. Med. Biol. **45**, 3721–3735 (2000)
89. Hall, R.M., Unsworth, A.: Friction in hip prostheses. Biomaterials **18**, 1017–1026 (1997)
90. Brockett, C., Williams, S., Jin, Z.M., Isaac, G., Fisher, J.: Friction of total hip replacements with different bearings and loading conditions. J. Biomed. Mater. Res. B Appl. Biomater. **81B**(2), 508–515 (2007)
91. Essner, A., Sutton, K., Wang, A.: Hip simulator wear comparison of metal-on-metal, ceramic-on-ceramic and crosslinked UHMWPE bearings. Wear **259**(7–12), 992–995 (2005)